Chaos, Solitons and Fractals 156 (2022) 111834

Contents lists available at ScienceDirect

Chaos, Solitons and Fractals

Nonlinear Science, and Nonequilibrium and Complex Phenomena

journal homepage: www.elsevier.com/locate/chaos

Multistable dynamics and control of a new 4D memristive chaotic Sprott B system

Ramesh Ramamoorthy[a], Karthikeyan Rajagopal[b], Gervais Dolvis Leutcho[c,d], Ondrej Krejcar[e,f], Hamidreza Namazi[e,g,*], Iqtadar Hussain[h]

[a] Centre for Artificial Intelligence, Chennai Institute of Technology, Chennai, India
[b] Center for Nonlinear Systems, Chennai Institute of Technology, Chennai, Tamilnadu 600069, India
[c] Department of Electrical Engineering, École de Technologie Supérieure (ÉTS), Montréal, Québec H3C1K3, Canada
[d] Research Unit of Laboratory of Condensed Matter, Electronics and Signal Processing (UR-MACETS) Department of Physics, Faculty of Sciences, University of Dschang, 67, Dschang, Cameroon
[e] Center for Basic and Applied Research, Faculty of Informatics and Management, University of Hradec Kralove, Hradec Kralove, Czechia
[f] University of Zilina, Univerzitna 1, 010 26 Zilina, Slovakia
[g] College of Engineering and Science, Victoria University, Melbourne, Australia
[h] Mathematics Program, Department of Mathematics, Statistics and Physics, College of Arts and Sciences, Qatar University, 2713, Doha, Qatar

ARTICLE INFO

Article history:
Received 24 September 2021
Revised 19 January 2022
Accepted 21 January 2022

Keywords:
Memristive Sprott B system
Rotational symmetry
Rotational symmetry broken
Coexisting of bifurcations
Partial amplitude control
Control of the multistability

ABSTRACT

This work proposes and investigates the dynamic behavior of a new memristive chaotic Sprott B system. One of the interesting features of this system is that it has a bias term that can adjust the symmetry of the proposed model, inducing both homogeneous and heterogeneous behaviors. Indeed, the introduced memristive system can turn from rotational symmetry (RS) to rotational symmetry broken (RSB) system in the presence or the absence of this bias term. In the RS system (i.e., absence of the bias term), pairs of symmetric attractors are formed, and the scenario of attractor merging is observed. Coexisting symmetric attractors and bifurcations with up to four solutions are perfectly investigated. In the RSB system (i.e., the bias term is non-zero), many interesting phenomena are demonstrated, including asymmetric attractors, coexisting asymmetric bifurcations, various types of coexisting asymmetric solutions, and period-doubling transition to chaos. We perfectly demonstrate that the new asymmetric/symmetric memristive system exhibits the exciting phenomenon of partial amplitude control (PAC) and offset boosting. Also, we show how it is possible to control the amplitude and the offset of the chaotic signals generated for some technological exploitation. Finally, coexisting solutions (i.e., multistability) found in the novel memristive system are further controlled based on a linear augmentation (LA) scheme. Our numerical findings demonstrated the effectiveness of the control technic through interior crisis, reverse period-doubling scenario, and symmetry restoring crisis. The coupled memristive system remains stable with its unique survived periodic attractor for higher values of the coupling strength.

1. Introduction

Recently, research works focused on the classification of attractors as either self-excited or hidden [1]. A self-excited attractor has a basin of attraction that is associated with unstable equilibrium. In contrast, a hidden attractor has a basin of attraction that does not intersect with small neighborhoods of any equilibrium points [2–4]. So, chaotic or periodic attractors that are associated with a system without any equilibrium points or with only stable equilibria are called hidden attractors [2–4]. Some of these findings are also obtained from memristive circuits designed based on the memristor theory [5]. It is considered as the fourth basic electronic element, aside from resistor, capacitor, and inductor. So far, memristors have been widely exploited to design a large number of circuits and systems, including chaotic circuits [6], nonvolatile memory [7], digital logic circuits [8], memristive neural networks, and memristive synapses [9]. Therefore, a large number of such systems have been introduced and investigated in the literature. Such investigations on chaotic systems are tied to various applications of chaotic systems in different engineering domains.

* Corresponding author at: Center for Basic and Applied Research, Faculty of Informatics and Management, University of Hradec Kralove, Hradec Kralove, Czechia.
E-mail address: hamidreza.namazi@monash.edu (H. Namazi).

https://doi.org/10.1016/j.chaos.2022.111834

Due to the existence of chaos in wide engineering fields, intensive studies lead to many areas of implementation related to chaotic systems [10–14]. Some examples of technological implementations of chaotic systems with either self-existed or hidden attractors are optimization [12], cryptography [15,16], artificial neural network [13], communication [11,17,18], random number generator [14], and image processing [10]. A good technic employed to design some novel chaotic systems was introducing the memristor equation in a three-dimensional (3D) system or a nonlinear feedback controller on a three-dimensional system. Both technics enable us to move from a 3D chaotic system to a 4D chaotic system.

In [19], a new autonomous 4D system without equilibrium, having two nonlinear quadratic terms, two adjustable coefficients, and seven terms, is studied. The system is constructed by using appropriate linear feedback control. Many interesting properties are found in the proposed system, including hyperchaos, quasi-periodic route to chaos, and coexisting stable states. A novel 4D chaotic system with infinite coexisting attractors is presented and investigated by Qiang et al. [20]. The proposed model is constructed by injecting a sinusoidal function into an existing 4D system. Therefore, infinite many coexisting attractors are proved numerically using phase diagrams and bifurcation diagrams. The circuit and microcontroller implementations of the model are carried out to confirm its concrete/physical meaning. In [21], the authors introduced a novel five-dimensional memristive hyperchaotic system with hidden behaviors. The proposed 5D system is constructed by introducing a flux-controlled memristor model into a well-known and improved 4D hyperchaotic system [22]. Coexisting attractors are discussed in the investigated model with their hidden extreme multistability. The hyperchaotic feature is experimentally confirmed. Hidden attractors are demonstrated numerically using Lyapunov exponents, bifurcation diagrams, and phase diagrams in a new 5D (five-dimensional) hyperchaotic Sprott B system [23]. The symmetry of the proposed model is used to prove coexisting hidden solutions in the proposed system. Very recently, Li et al. [24] proposed a novel 4D hyperchaotic memristor system by introducing a magneton memristor into the 3D chaotic Sprott B system. The hyperchaotic behaviors of the proposed memristor system are demonstrated using dissipation, Lyapunov exponent, and stability. A novel memristive Hindmarsh-Rose (HR) neuron model with electromagnetic induction was designed [25]. The model was constructed by introducing an ideal flux-controlled memristor with cosine memductance [26] into the classical HR neuron model to characterize the electromagnetic field effects on neurons. Therefore, hidden homogeneous extreme behaviors were generated. Constructed chaotic systems with rich dynamical properties (e.g., extreme multistability, offset boosting, coexisting attractors, amplitude control, and symmetry) are discussed [27–32]. To the best of the authors' knowledge, it is observed from Table 1 that no chaotic/hyperchaotic memristor Sprott B system with self-excited attractors was reported in the literature. Also, this table highlights the property of some 4D or 5D Sprott B systems proposed within this work.

In particular, a chaotic signal is one positive Lyapunov exponent (LE) fingerprint in a nonlinear dynamical system. However, if a nonlinear system has more than one positive LE, the generated signal will be hyperchaotic. In 1994, Sprott constructed nineteen different simple three-dimensional (3D) chaotic systems with both two quadratic nonlinear elements and five terms [33]. The memristor equation is introduced to obtain a novel 4D chaotic system with striking properties considering the chaotic Sprott B system. One of the interesting features of this system is that it has a bias term that can adjust the symmetry of the proposed model, inducing both homogeneous and heterogeneous behaviors. Recall that in [34], by replacing the offset boosting parameter in Sprott M chaotic system with a periodic function, infinitely many co-existing homogeneous attractors are investigated. Therefore, a chaotic signal with either polarity can be obtained by selecting different initial conditions. A field programmable analog array (FPAA) was used to construct a programmable chaotic circuit, and the predicted attractors were observed on an oscilloscope. In this paper, we proposed a novel four-dimensional chaotic Sprott B system without any periodic function compared to the previous work. We show both homogeneous and heterogeneous solutions in some oscillations modes. In the RS case (i.e., the bias term is zero), pairs of symmetric attractors are viewed, and the scenario of attractor merging is analyzed. Coexisting symmetric attractors and bifurcations with up to four solutions are studied. Furthermore, in the RSB model (i.e., the bias term is non-zero), many important phenomena are demonstrated, including asymmetric attractors, coexisting asymmetric bifurcations, various types of coexisting asymmetric solutions, and period-doubling transition to chaos. We perfectly demonstrate that the new memristive system exhibits the exciting phenomenon of partial amplitude control (PAC) and offset boosting. Also, we show how it is possible to control the amplitude and the offset of the chaotic signals generated for some technological exploitation. The technic of linear augmentation is also applied to control the coexistence of up to four different symmetrical attractors. We recall that technics of the linear augmentation has been already used to control the coexistence of the attractors in several classes of the nonlinear dynamical systems among which a model of coupled Hindmarsh–Rose neuron [35], Hopfield neural network [36], chaos, and Hyperchaos Chua's oscillator [16,37], Hyper-jerk oscillator [38], to name a few [39,40]. However, more examples of systems, including memristive ones with coexisting attractors, need to be investigated based on this control technique, hence the interest of this work.

This work's plan is presented as follows: In Section 2, the combination of the memristor equation and the Sprott B system enables obtaining the novel 4D autonomous system. In Section 3, the bifurcations exhibited by the introduced system are analyzed. In Section 4, the multistable behavior of the model involving the coexistence of the multiple stables is explored. In Section 5, the phenomenon of the offset and amplitude control is addressed. In Section 6, the control of the coexistence of the multiple stable states is addressed through the linear augmentation method. Finally, we summarize the paper in Section 7.

2. Model of the new 4D memristive chaotic system

In 1994, Sprott constructed nineteen different simple three-dimensional (3D) chaotic systems with both two quadratic nonlin-

Table 1
Categorization of reported 4D or 5D Sprott B systems with various characteristics.

Nature of the system	Type of coupling	Amplitude and offset control	Number of coexisting attractors	Type of attractors	Multi-stability control	Refs.
5D hyper-chaotic	Nonlinear feedback	–	02	Hidden	–	[23]
4D chaotic	Nonlinear feedback	–	Infinite	Hidden	–	[20]
4D hyper-chaotic	Memristor	–	–	Hidden	–	[24]
4D chaotic	Memristor	Yes	02, 03, and 04	Self-excited	Yes	This work

ear elements and five terms [33]. The chaotic Sprott B system is expressed by the following first-order, autonomous, ODE (ordinary differential equations)

$$\begin{cases} \dot{x}_1 = x_2 x_3 \\ \dot{x}_2 = x_1 - x_2 \\ \dot{x}_3 = 1 - x_1 x_2 \end{cases} \tag{1}$$

When a memristive device equation is introduced into Eq. (1), a new 4D system construct from the Sprott B model is obtained

$$\begin{cases} \dot{x} = ryz + g \\ \dot{y} = x - y \\ \dot{z} = 1 - mW(u)xy \\ \dot{u} = axy - u \end{cases} \tag{2}$$

In Eq. (2), all the parameters are positive. Also, the relation between the current and the voltage of the memristive device is given by Eq. (3).

$$\begin{cases} i_m = W(u)v_m \\ W(u) = \alpha + \gamma|u| + \beta u^2 \\ \dot{u} = kv_m - u \end{cases} \tag{3}$$

where the coefficients values are $\alpha = 1$, $\beta = 0.05$, $\gamma = 0.5$, $m = 11$, $a = 1$, $g = 0.0$ and $r = 3$. Recall that in Eq. (3), α, β, and γ are intrinsic coefficients of the memristive device. The memristor Eq. (3) was first introduced by Zang et al. [31]. In this paper, a novel 4D chaotic system is constructed by modifying the 3D chaotic Sprott B system, using the memristor model (3). In system (2), the bias term g breaks the rotational symmetry of the model completely. That is, in the absence of the bias term (i.e., $g = 0$), rotational symmetry is observed, and thus our model (2) remains undisturbed under the change $(x, y, z, u) \to (-x, -y, z, u)$. This symmetry property is exploited to generate pairs of symmetric chaotic attractors and their corresponding Poincaré sections as presented in Fig. 1 in different phase planes. Such a transformation of state variables (i.e., symmetry) has been effectively used to prove the existence of bistability (i.e., the presence of a pair of mutually symmetrical solutions/attractors) in the memristive T chaotic system [31]. Next, when $g \neq 0$, the previous symmetry can no longer be discussed since the novel 4D system does not obey the transformation $(x, y, z, u) \to (-x, -y, z, u)$. This case refers to RSB, which is rarely discussed in chaotic systems with memristor. This situation (i.e., breaks the symmetry) makes the system (2) more general.

In addition, the evaluation of the volume contraction rate of the model enables to obtain Eq. (4).

$$\mathrm{div}V = \nabla \cdot V = \begin{pmatrix} \partial/\partial x \\ \partial/\partial y \\ \partial/\partial z \\ \partial/\partial u \end{pmatrix} \cdot \begin{pmatrix} ryz + g \\ x - y \\ 1 - mW(u)xy \\ axy - u \end{pmatrix} = -2 \tag{4}$$

Since $\nabla V < 0$, we can conclude that the introduced 4D model is dissipative. Then, it will be able to support chaotic stable states.

2.1. Equilibrium points and their stability

The equilibria of the novel memristive system investigated in this work are obtained by solving the following equations

$$\begin{cases} 0 = ryz + g \\ 0 = x - y \\ 0 = 1 - mW(u)xy \\ 0 = axy - u \end{cases} \tag{5}$$

After some algebraic manipulation, it is found that the equilibria of our model are given by

$$E(x^*, y^*, z^*, u^*) = \left(\pm\sqrt{\frac{u}{a}}, \pm\sqrt{\frac{u}{a}}, \; -\left(\pm\frac{g}{r}\sqrt{\frac{a}{u}} \right), \; u \right) \tag{6}$$

where $u$is obtained by solving the transcendental equation

$$1 - m\left(\alpha + \gamma|u| + \beta u^2\right)\frac{u}{a} = 0 \tag{7}$$

Indeed, any equilibrium point provided in Eq. (6) is obtained by solving the transcendental Eq. (7). However, the numerical solution of this transcendental equation obtained in Table 1 shows a unique value of u ($u = 0.08711157266$) for the fixed set of parameters α, β, γ, m, and a. Also, $0 < u < 1$.

For model given in Eq. (2), the Jacobian matrix is obtained by the linear analysis of the system at the equilibrium point as

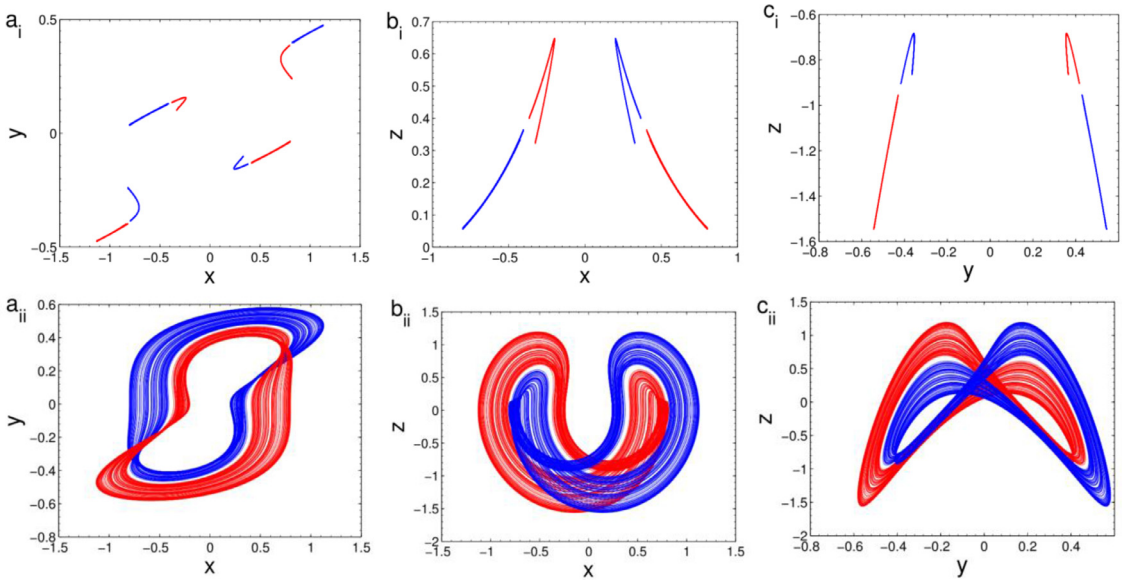

Fig. 1. Coexisting pairs symmetric attractors in system (2) when $r = 4.85$ with initial values $IC = (0.5, 0.2, 0.1, 0.1)$ for blue and $(-0.5, -0.2, 0.1, 0.1)$ for red: a(i)-(ii) Poincaré section and phase diagram in $(x - y)$ plane, b(i)-(ii) Poincare section and phase diagram in $(x - z)$ plane and c(i)-(ii) Poincare section and phase diagram in $(y - z)$ plane. The parameters are the same as in Fig. 1.

follows:

$$J=\begin{bmatrix} 0 & rz^* & ry^* & 0 \\ 1 & -1 & 0 & 0 \\ -my^*\left(\alpha+\gamma|u^*|+\beta u^{*2}\right) & -mx^*\left(\alpha+\gamma|u^*|+\beta u^{*2}\right) & 0 & -mx^*y^*(\gamma \mathrm{sign}(u^*)+2\beta u^*) \\ ay^* & ax^* & 0 & -1 \end{bmatrix} \tag{8}$$

The stability of the model is obtained by analyzing the sign of the characteristic equation obtained by solving Eq. (9).

$$\lambda^4+m_1\lambda^3+m_2\lambda^2+m_3\lambda+m_4=0 \tag{9}$$

With

$$\begin{aligned} m_1 &= 2 \\ m_2 &= (-ry^*J_{31}-rz^*+1) \\ m_3 &= \left(-ary^{*2}J_{34}-2ary^*J_{31}-ry^*J_{32}-rz^*\right) \\ m_4 &= -arx^*y^*J_{34}-ry^*J_{31}-ry^*J_{32} \\ J_{31} &= -my^*\left(\alpha+\gamma|u^*|+\beta u^{*2}\right) \\ J_{32} &= -mx^*\left(\alpha+\gamma|u^*|+\beta u^{*2}\right) \\ J_{34} &= -mx^*y^*(\gamma sign(u^*)+2\beta u^*). \end{aligned} \tag{10}$$

The coefficients of the polynomial Eq. (9) are all nonzero. Based on the Routh–Hurwitz criterion, the real parts of the roots of Eq. (9) are positive if and only if inequalities of Eq. (11) are satisfied:

$$\begin{aligned} m_1 &> 0 \\ m_1m_2-m_3 &> 0 \\ m_1(m_2m_3-m_1m_4)-m_3^2 &> 0 \\ m_4 &> 0 \end{aligned} \tag{11}$$

Based on those inequalities, the stabilities of the model around some equilibrium points are discussed in Table 2.

2.2. Kaplan-Yorke dimension

when $\alpha=1, \beta=0.05, \gamma=0.5, m=11, a=1, g=0.0$ and $r=3$, the new 4D memristive system exhibit a chaotic oscillation (see Fig. 2) with Lyapunov exponents (LEs): $L_1=0.3140, L_2=0.0023, L_3=-1.0394$ and $L_4=-1.2769$. According to the above values of the LEs, we can notice that:

$$\sum_{i=1}^{2}L_i=0.3163>0 \; and \; \sum_{i=1}^{3}L_i=-0.7231<0$$

The Kaplan-Yorke dimension or the Lyapunov dimension of the new 4D chaotic Sprott B system (2) is defined as

$$D_{KY}=j+\frac{1}{|L_{j+1}|}\sum_{i=1}^{j}L_i, \tag{12}$$

where j is the largest integer verifying $\sum_{i=1}^{j}L_i\geq 0$ and $\sum_{i=1}^{j+1}L_i<0$. Therefore, we obtained

$$D_{KY}=2+\frac{0.3163}{|-1.0394|}=2.3043. \tag{13}$$

3. Bifurcation and attractor merging

The nonlinear system dynamics can be characterized numerically by using appropriate nonlinear tools, including phase diagram, Lyapunov exponent (LE), time series, Poincare section, frequency spectra, and basin of attraction, to name a few. However, a bifurcation diagram is currently used to summarize all the dynamical features of the model in an appropriate range of control parameters. In some cases, the bifurcation diagram is used to explain the bursting mechanism. Indeed, a bifurcation diagram can be obtained by sweeping the control parameter in upward and backward directions. Such technic can help to capture hysteresis and other complex phenomena. The interesting phenomenon of antimonotonicity (i.e., creation of annihilation of periodic orbit via reserve period-doubling sequence) is widely demonstrated by exploiting bifurcation diagrams. In this section, we use the bifurcation graphs, the phase diagrams, and the basin of attraction to characterize the dynamics of the new 4D memristive chaotic system in the symmetric and asymmetric mode of oscillations by showing how the symmetry property allows merging a pair of symmetric attractors into an asymmetric attractor.

When the dissymmetry parameter $g=0$, the bifurcation diagram (resp. the Lyapunov exponent's spectrum) of the system (2) is plotted as shown in Fig. 3a (resp. Fig. 3b). Indeed, the peak values of the variable x are drawn by first saving them in a file. By

Table 2
fixed point of the introduced model and their stability for some values of the control parameters when $\alpha=1$, $\beta=0.05$, $\gamma=0.5$, $m=11$, $a=1$.

Control parameters	Equilibrium points $E(x^*,y^*,z^*,u^*)$	Eigenvalues and stability
$g=0$ and $r=3$	(0.2951466969; 0.2951466969; 0; 0.08711157266)	$0.3885\pm1.8222i$ $-1.7448+0.000i$ $-1.0321+0.000i$ Unstable saddle-foci
	(−0.2951466969; −0.2951466969; 0; 0.08711157266)	$0.1973\pm2.0917i$ $-1.3289+0.000i$ $-1.0657+0.000i$ Unstable saddle-foci
$g=0.03$ and $r=5.22$	(0.2951466969; 0.2951466969; −0.01947210149; 0.08711157266)	$0.3885\pm1.8222i$ $-1.7448+0.000i$ $-1.0321+0.000i$ Unstable saddle-foci
	(−0.2951466969; −0.2951466969; 0.01947210149; 0.08711157266)	$0.1973\pm2.0917i$ $-1.3289+000i$ $-1.0657+0.000i$ Unstable saddle-foci

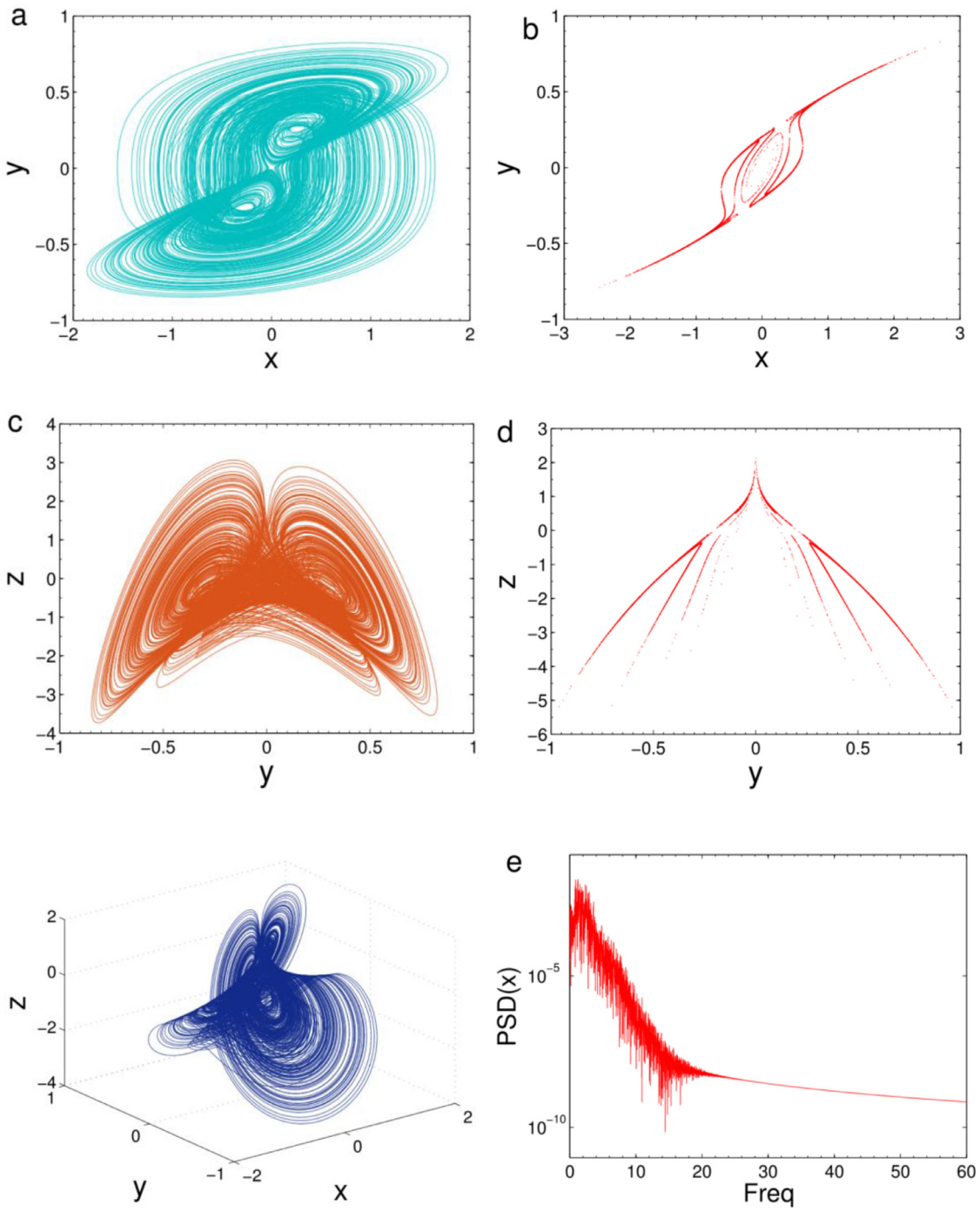

Fig. 2. The chaotic oscillation of system (2) with $r = 3, \alpha = 1, \beta = 0.05, \gamma = 0.5, m = 11, a = 1, g = 0$ and initial values $(0.5, 0.2,\ 0.1,\ 0.1)$: (a) phase trajectorie in $(x - y)$; (b) Poincaré section in $(x - y)$; (c) phase trajectorie in $(y - z)$; (d) Poincare section in $(y - z)$; 3D view in (x, y, z) and (e) frequency spectrum.

increasing (resp. decreasing) the control parameter r from $_{1.5}$ to $_{6}$ with symmetric initial points $(\pm 0.5,\ \pm 0.2,\ 0.1,\ 0.1)$, the graph in black (resp. in magenta) is gained, indicating the scenario observed in our model. By analyzing the LEs spectrum of Fig. 3b, two distinct dynamics can be categorized (i.e., chaotic behavior and periodic behavior). From 1.5 to 2.4, and 2.6 to 5.2, the first LE (i.e., L_1) is positive, the second LE (i.e., L_2) is zero, and the last two LEs (i.e., L_3 and L_4) are always negative. It is the chaotic regime of the 4D system. However, we can note a small periodical window in this chaotic zone where the first and second LEs are zero. In addition, when $r\varepsilon]5.2, 6]$, the nonlinear oscillator operates entirely in its regular area. The LEs spectrum correctly demonstrates the observed bifurcation sequence when the coefficient r is swept upward. The detailed results presented in Fig. 4 show that when $r = 6$, system (2) exhibits a symmetric pair of period-1 limit cycles solutions in the (x, z) plane, and these periodic cycles solutions experience a series of period-doubling as r is decreased, reaching to a symmetric pair of chaotic solution at $r = 5.1$. One can easily observe that under the critical value $r = 5.1$, the size of the chaotic attractor grows, touching each other along their edges, inducing/creating at $r = 4.55$ a unique symmetric strange chaotic attractor. At $r = 4.822$, the attractors are thoroughly entangled notwithstanding remaining in separate demarcation regions (i.e., basins of attraction). Before the merging, the two chaotic solutions present a complex fractal

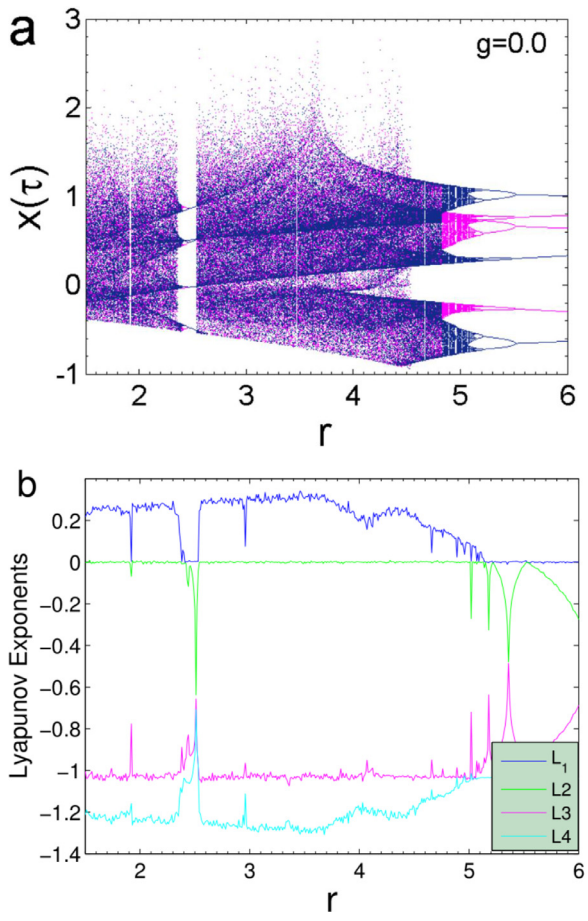

Fig. 3. Bifurcation diagrams of x and Lyapunov exponents versus r of system (2) when $1.5 \leq r \leq 6$ plotted in upward (black) and backward (magenta) directions with symmetric initial values $(\pm 0.5,\ \pm 0.2,\ 0.1,\ 0.1)$ for $\alpha = 1, \beta = 0.05, \gamma = 0.5, m = 11, a = 1$.

basin boundary. This demarcation region of IC is shown in Fig. 5a. In this case, a perfect symmetry of the attractors is observed.

However, the cross-section of the demarcation regions of ICs when the two attractors are completely merged (resp. when the single asymmetric attractor is formed) are shown in Fig. 5b (resp. Fig. 5c). When $g \neq 0$, the system (2) loses its symmetry property, and no possible attractor merging is found in the model. In other words, all the attractors in the system are asymmetric, and the dynamic of the proposed model becomes more complex. A parallel branch appears in the symmetric bifurcation region, as shown in Fig. 6a for $g = 0.03$. This bifurcation graph shows a wide area of chaotic oscillation with $r\varepsilon[1.5, 4.5]$, which is well confirmed by its Lyapunov exponent's spectrum depicted in Fig. 6b. However, in the region $r\varepsilon[5.2, 6]$, we can see the transition to chaos correlating with the parallel branch (see Fig. 6a) when decreasing the control parameter r. The sequence period-2 limit cycle $\rightarrow$ period-4 $\rightarrow$ chaos $\rightarrow$chaos illustrated by the 3D phase diagrams of Fig. 7 confirm well the previous scenario revealed by the bifurcation diagram. It is important to note that the apparition of the parallel branch on Fig. 6a originates the coexisting asymmetric solutions, which is more reviewed in the next section.

4. Coexisting bifurcation diagrams and multistability

4.1. Case $g = 0$

The bifurcation diagram shown in Fig. 3 illustrated interesting phenomena (e.g., chaos, periodic orbits, attractor merging, symmetric bifurcation, and period-doubling) when the control coefficient r varied upward or backward directions from 1.5 to 6.0. These behaviors are generally studied in nonlinear dynamical systems, including memristor oscillator [29,41–43], Chua's circuit [37], series hybrid electric vehicle (SHEV) [44,45], Lorent and Lü systems [46–48], and hyperjerk systems [49–51], to name a few [52,53]. About these behaviors, multistability remains a hot and exciting topic in nonlinear dynamics. This interesting feature has been very recently revealed for the first time in series hybrid electric vehicles [44], with the coexistence of up to three disconnected solutions. This subsection aims to investigate such striking phenomenon of multiple coexisting attractors/solutions or coexisting bifurcations diagrams. Fig. 8 presents the coexisting bifurcations branches of the system (2) in the region $r\varepsilon[4.95, 4.99]$. These coexisting branches are obtained by scanning the coefficients r in the upward (i.e., black and blue) and backward (i.e., magenta and red) directions with symmetric initial conditions as indicates in each data. In Fig. 8, when $r\varepsilon[4.9609, 4.9801]$, one can find up to four coexisting branches (i.e., two period-3 branches and two chaotic branches). This region demonstrates a possible existence of four disconnected symmetric solutions in the system (2) when fixing all the system parameters and selected random initial values.

4.2. Case $g \neq 0$

Considering the same bifurcation diagram of Fig. 6 (i.e., when $g = 0.03$), we capture it zoom in the region $r\varepsilon[5,\ 6]$ as shown in Fig. 9. This Figure demonstrates an interesting scenario when the coefficient r is varied. In particular, from 5.2 to 5.84, we note the coexistence of two different branches in this specific range of the control parameter. That is, a period-1 branch (blue) obtains in the upward direction coexists with a chaotic branch (red) gets in the download direction when $g = 0.03$. Since the model operates here in an asymmetric mode of oscillation, the coexisting solutions in this region will always be asymmetric, which is the pure characteristic of heterogeneous solutions. The results of this demonstration are provided in Fig. 10 through different phase diagrams plotted in the $(y,\ z)$ plane. It is important to mention that all these coexisting solutions are obtained by fixing all the system coefficients/parameters but using random ICs. For instance, when $r = 5.22$, two arbitrary initial points enable the coexistence of the couple (period-1, chaos). At $r = 5.69$, an asymmetric period-1 limit cycle attractor coexists with a chaotic period-3 solution (see Fig. 10b).

Similarly, when $r = 5.55$, an asymmetric period-1 orbit coexists with chaotic period-2 attractors, as shown in Fig. 10c. The cases in Figs.10d and 10e also demonstrate that two distinct limit cycle attractors can coexist. It can be seen that an asymmetric period-4 orbit or an asymmetric period-2 orbit coexists with the same period-1 limit cycle. The associating cross-section of the basin of attraction in the same phase plane is shown in Fig. 10f. To our best knowledge, it is rarely found in the literature such combination of coexisting heterogeneous solutions where a sequence of period-doubling coexists with a single periodic orbit. The enlargement of the diagram of Fig. 9 in the interval $r\varepsilon[5.34,\ 5.4]$ is shown in Fig. 11. This figure presents the region of the parameter r where different bifurcation branches coexist in the system. One can observe a good illustration of the coexistence of three distinct asymmetric branches of solutions consisting of a period-1 family (green), the chaotic branch (red), and the period-3 branch that exhibit a sequence of PD route to chaos when r is scanning in a downward direction (i.e., decreasing). A perfect coexistence of three different asymmetric attractors confirms these coexisting bifurcations, as shown in Figs. 12, and 13. The case presented in Fig. 13b demonstrates a magnetization of the three coexisting so-

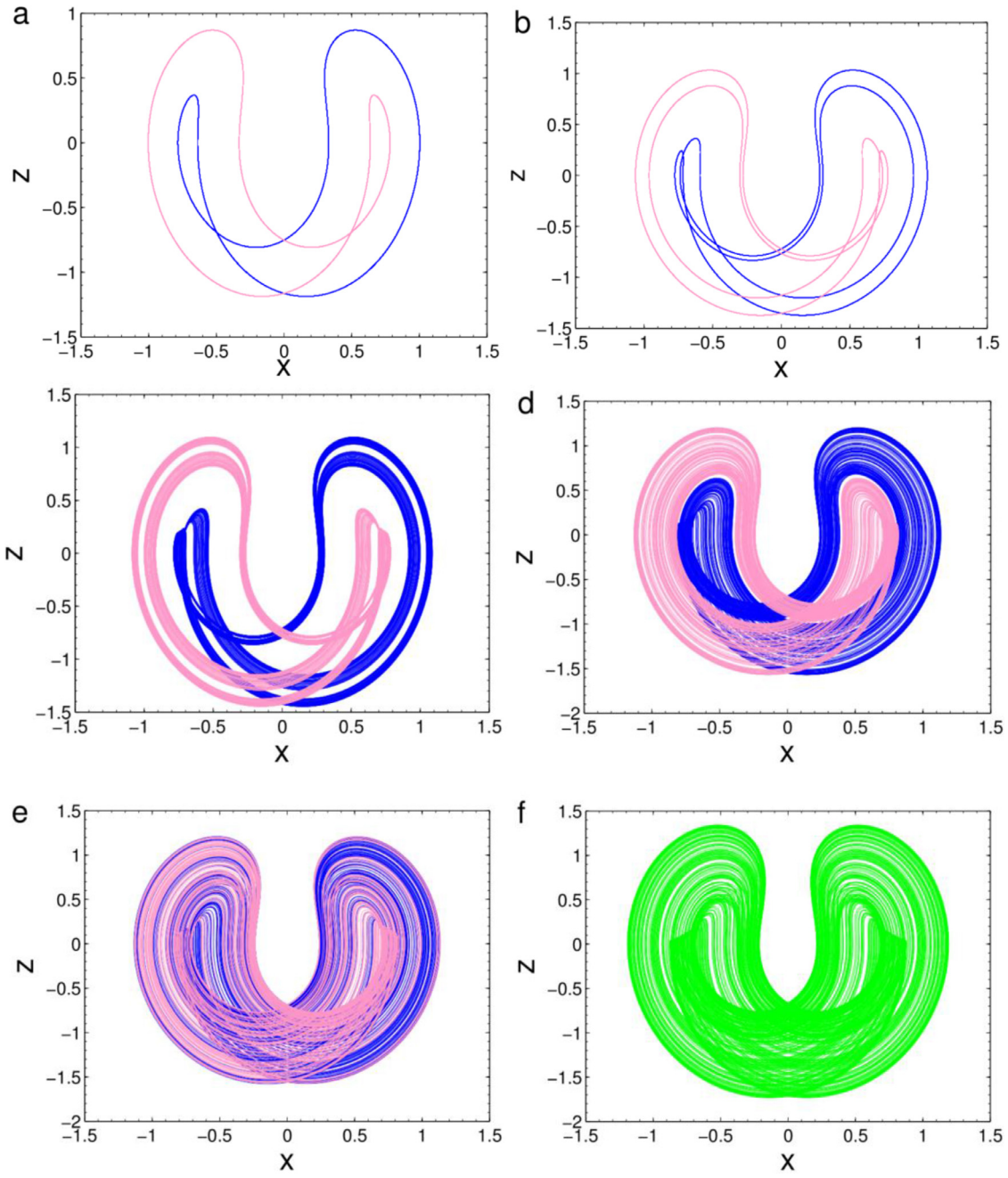

Fig. 4. Senario of attractor merging via period-doubling to chaos in system (2) for $r = 6.0, r = 5.3, r = 5.1, r = 4.838, r = 4.822$ and $r = 4.55$, respectively. The rest of system parameters are $\alpha = 1, \beta = 0.05, \gamma = 0.5, m = 11, a = 1, g = 0, IC1 = (-0.5, -0.2,\ 0.1,\ 0.1)$ for Blue attractors and $IC2 = (0.5, 0.2,\ 0.1,\ 0.1)$ for orange and green attractors.

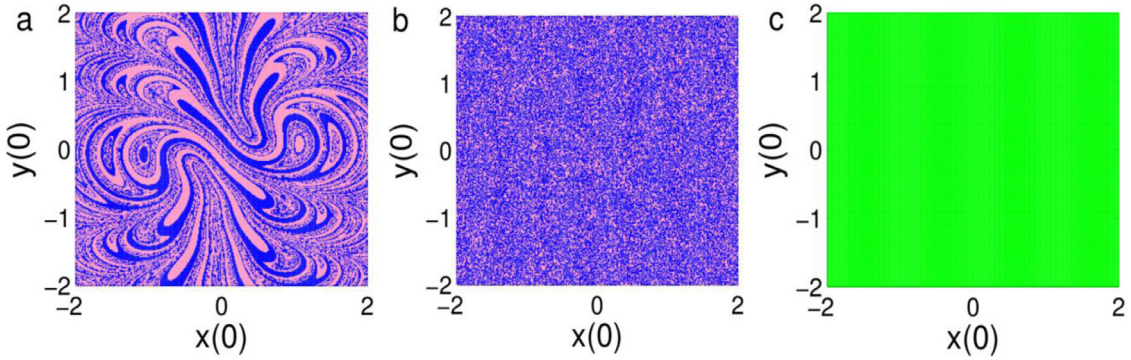

Fig. 5. Cross section of the basin of attraction showing the phenomenon of attractor merging in $[x(0) - y(0)]$ when $z(0) = u(0) = 0.1$: (a) $r = 4.838$, (b) $r = 4.822$ and (c) $r = 4.55$.

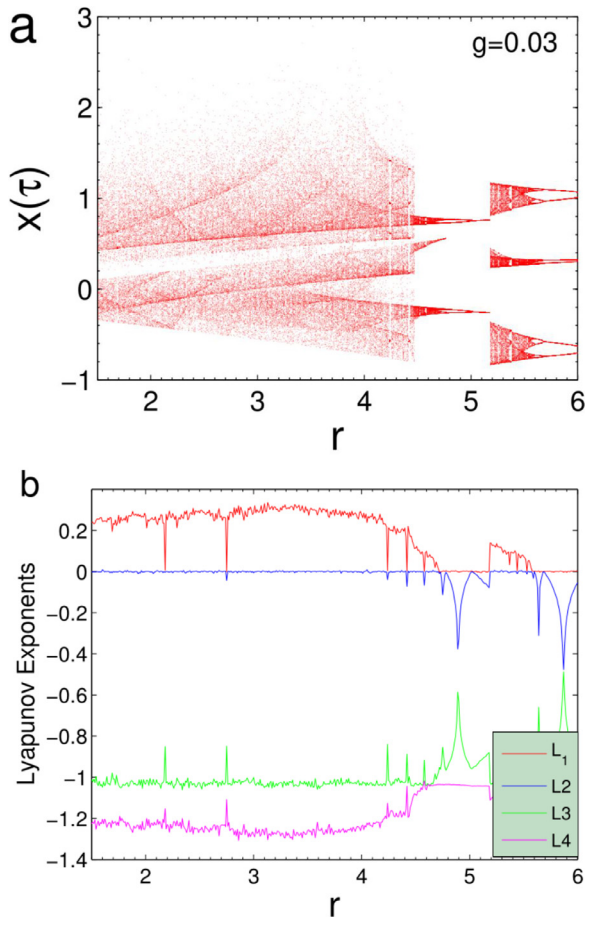

Fig. 6. Bifurcation diagrams of x and Lyapunov exponents versus r of system (2) when $1.5 \leq r \leq 6$ plotted in upward direction with initial value (0.5, 0.2, 0.1, 0.1) for $\alpha = 1, \beta = 0.05, \gamma = 0.5, m = 11, a = 1$.

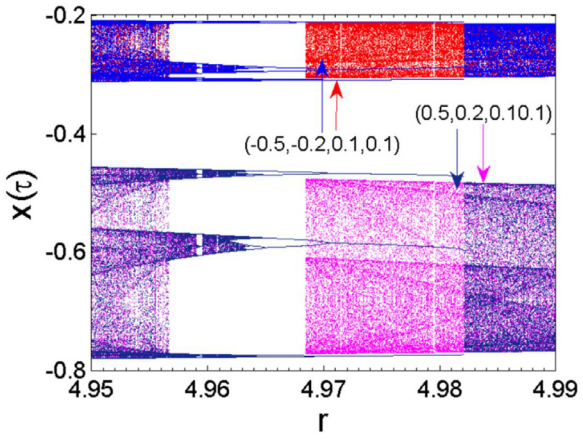

Fig. 8. Zoom of the bifurcation diagram of Fig. 3 in the interval $r\varepsilon[4.95, 4.99]$ using upward and backward directions with symmetric *ICs*. The region of four coexisting dynamics can be visualized in the zone $r\varepsilon[4.969, 4.981]$.

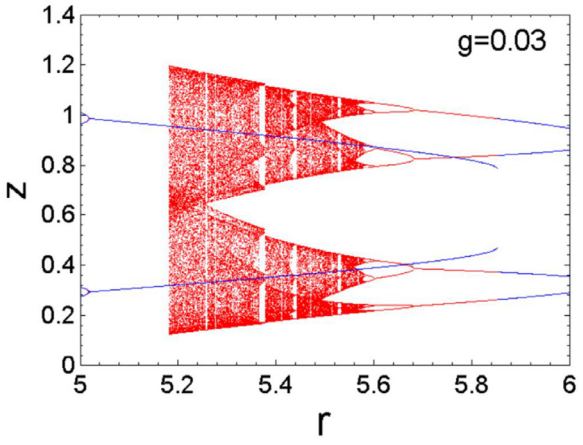

Fig. 9. Coexisting bifurcations diagrams obtained in the same regions of parameter $r(5 \leq r \leq 6)$ plotted in the upward (blue) and backward (red) directions with same $IC = (0.5, 0.2, 0.1, 0.1)$ for $\alpha = 1, \beta = 0.05, \gamma = 0.5, m = 11, a = 1$.

lutions in a demarcation region with three different colors illustrating each attractor found.

5. Offset and amplitude control

5.1. Offset boosting control

A chaotic signal can be moved in phase space for a variable boostable system by adding a constant to a single variable that appears to the system. If the attractor is shifted in the phase space, its basin of attraction will be relocated to remain in the attractor zone. In a chaotic system, variable boostable can be used to create coexisting attractors (i.e., multistability). An introduction of a boosting controller in a symmetric system breaks this symmetry without changing its attractors' nature. As discussed by Li and

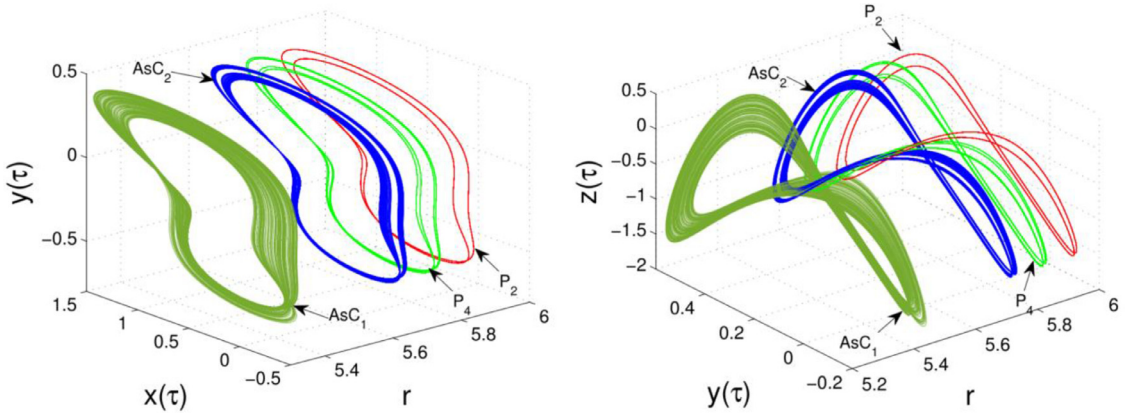

Fig. 7. 3D view of the transition to chaos in the asymmetric system (2) when $g = 0.03$: the emergence to chaos is observed by the sequence period-2 → period-4 → chaos → chaos when varying r from 5.4 to 6 with initial point $IC = (0.5, 0.2, 0, 0)$.

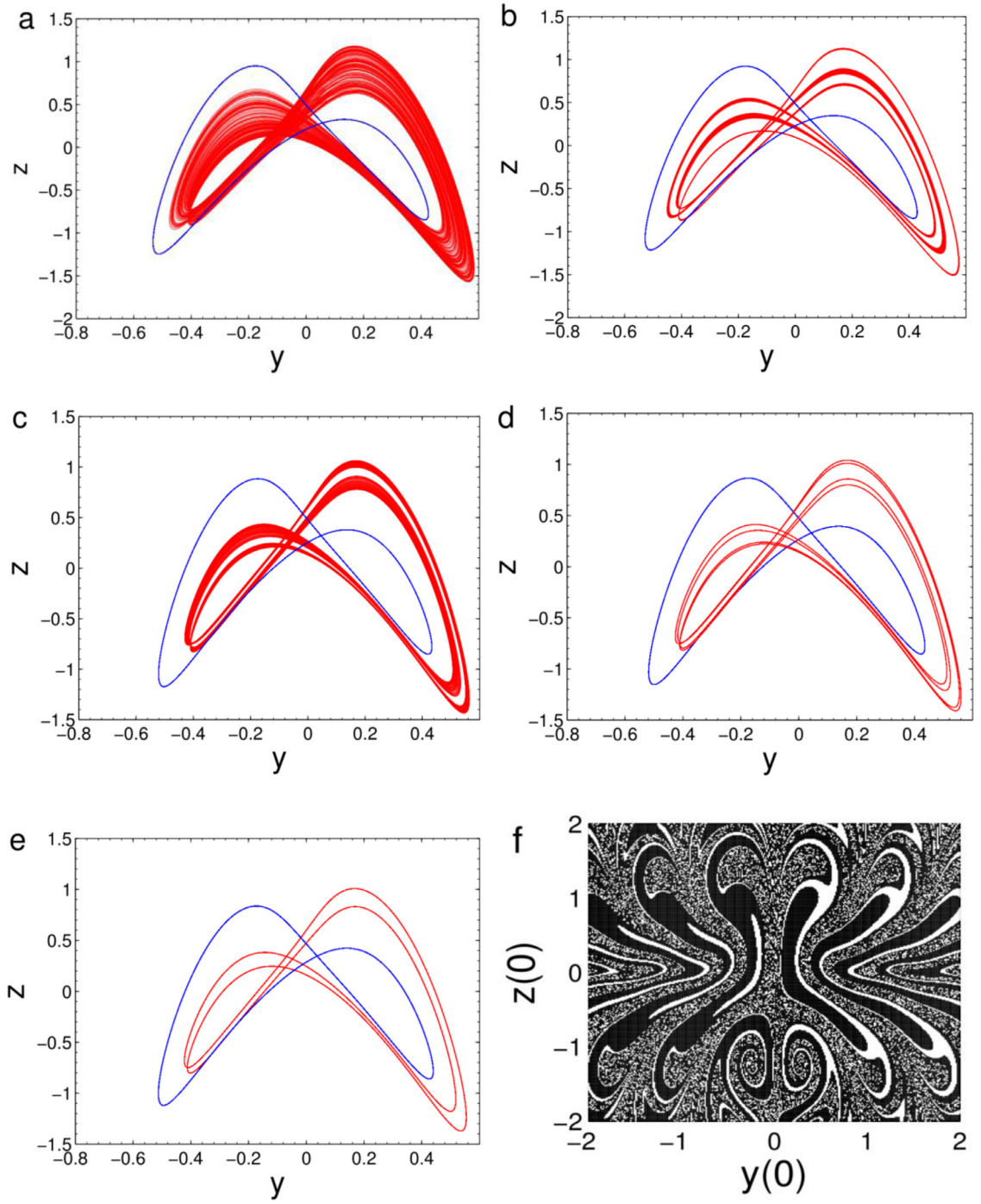

Fig. 10. Coexisting asymmetric attractors (when $g = 0.03$) for the same parameters setting in Fig. 6. The initial value corresponding to the red attractor is $IC1 = (0.5,\ 0.2,\ 0,\ 0)$: (a) $r = 5.22$ with $IC2 = (5,\ 0.2,\ 0,\ 0)$, (b) $r = 5.69$ with $IC2 = (1,\ 0.2,\ 0,\ 0)$, (c) $r = 5.55$ with $IC2 = (0.36,\ 0.2,\ 0,\ 0)$, (d) $r = 5.63$ with $IC2 = (0.36,\ 0.2,\ 0,\ 0)$, and (e) $r = 5.75$ with $IC2 = (0.36,\ 0.2,\ 0,\ 0)$. (f) The magnetization space of initial values in $(y(0) - z(0))$ plane for $r = 5.75$ when $x(0) = u(0) = 0$. Black region for red attractor and while region for blue attractor.

Sprott in [54], examples of chaotic flows that provide offset boosting by a single constant in the governing equations are presented. The authors combine offset boosting with amplitude control to perform a wide range of signals without affecting their dynamic properties, such as Lyapunov exponents and power spectra. They also demonstrate that offset boosting in symmetric systems can keep bistability. The offset-boosted symmetric system can also provide a symmetric pair of coexisting attractors in coordinate-shifted basins of attraction. In the same line, a simple chaos generator of conditional symmetry induced by offset boosting is investigated using an efficient methodology of dynamics editing in [55]. A novel hyperbolic function flux-controlled memristor chaotic system with conditional symmetry, capable of showing attractor growing, is discovered [56]. The proposed nonlinear system was designed based on an existing offset-boostable chaotic system. By exploiting the variable boostable in a sprott B system, infinitely many coexisting periodic or chaotic solutions are generated using single sinusoidal nonlinearity [57]. Exploiting the transformation of the vari-

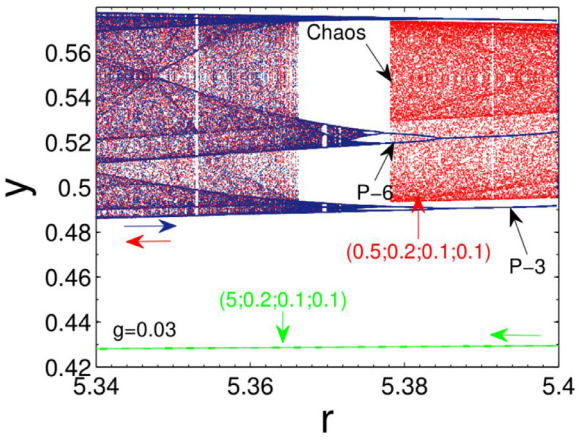

Fig. 11. Coexisting bifurcations diagrams obtained in the same regions of parameter $r(5.34 \leq r \leq 5.4)$ for $g = 0.03$. The rest of parameters are $\alpha = 1, \beta = 0.05, \gamma = 0.5, m = 11, a = 1$.

able $z \to z + \delta$ and substituting it into the new 4D system given in Eq. (2), yields

$$\begin{cases} \dot{x} = ry(z+\delta) + g \\ \dot{y} = x - y \\ \dot{z} = 1 - mW(u)xy \\ \dot{u} = axy - u \end{cases} \tag{14}$$

When we fix all the system parameters as those in Fig. 1, and by varying the boosting-controller δ, we obtained phase diagrams with attractors that can shift in the z-direction. Clearly, a positive value of δ shifts attractor negatively in the z-direction while a negative value of δ shifts attractor in the positive z-direction, as shown in Fig. 14. Fig. 14(a) is the 2D view of offset boosting realized in the $(y,\ z)$ plane and Fig. 14(b) is obtained in the 3D view in $(z,\ y,\ x)$ plane when $\delta\varepsilon[-5,\ 0,\ 5]$ and initial point $IC = (1,\ 0.2,\ 0,\ 0)$.

5.2. Partial amplitude control (PAC)

Recall that amplitude control modulation can be achieved in dynamical system through an appropriat choice of the coeficients of the absolute value or quadratic terms. In partial amplitude control (PAC), the amplitude modulation parameter controls the amplitude of some system variables linearly compared to total amplitude control (TAC), where all the system's variables are modulated simultaneously [58–60]. Besides, in both situations (i.e., PAC or TAC), the Lyapunov exponent (LE) spectrum remains constant. We can examined such interesting property in our new memristive chaotic system (2).

Suppose the following transformation of variables when $g = 0.0$

$$x = \sqrt{\eta}\hat{x},\ \ y = \sqrt{\eta}\hat{y}, z = \hat{z}, u = \hat{u} \tag{15}$$

By substituting Eq. (15) into Eq. (2), we derive a new ODE in terms of the state variable $\hat{x}, \hat{y}, \hat{z}$, and $\hat{u}$ as

$$\begin{cases} \dot{\hat{x}} = r\hat{y}\hat{z} \\ \dot{\hat{y}} = \hat{x} - \hat{y} \\ \dot{\hat{z}} = 1 - \eta mW(\hat{u})\hat{x}\hat{y} \\ \dot{\hat{u}} = a\eta\hat{x}\hat{y} - \hat{u} \end{cases} \tag{16}$$

where the nonlinear function $W(\hat{u})$ is given in Eq. (3). It can be seen that the coefficients m and a are the phase reversal parameters of the system (16).

These parameters can therefore amplify the two variables x and y nonlinearly. Controlled the signal's amplitude of the 4D memristive system (16), amounts to adjusting the coefficient η. Accordingly, the outputs chaotic signals $x(\tau)$ and $y(\tau)$ will be rescaled according to $1/\eta$. When $\eta\varepsilon[0,\ 25]$, the amplitudes evolvement of states x and y are capture as shown in Fig. 15a. Their corresponding bifurcation diagrams of the local maxima x and y presented in Fig. 15b, c confirm well the amplitude rescaling. It is observed that when η varied from $\eta = 0$ to $\eta = 25$, the amplitude of the outputs signal x and y are typically controlled according to $1/\eta$ but keeping the LEs values as shown Fig. 15d. Partial amplitude control is also confirmed using phase diagrams as depicted in Fig. 16a, c in (x, y) and $(y,\ u)$ planes. The amplitude of the chaotic signal decrease when increasing the controller η. It can be seen in Fig. 16a that the amplitudes chaotic signals x and y are controlled simultaneously, while in Fig. 16c, the amplitude signals of u are not modified/affected. Fig. 16b indicates that offset boosting and amplitude control can be perfectly achieved.

6. Control of multistable dynamics in the Sprott B system based on linear augmentation (LA) scheme

6.1. Brief description on the control method

The control scheme study in this section helps us suppress one or more coexisting attractors found in the multistable region of the Sprott B model. Clearly, the strategy help to moves from a multistable system to a monostable one by introducing a simple linear feedback control to the original system (2). The multistable system can be therefore controlled by adjusting a specific coefficient

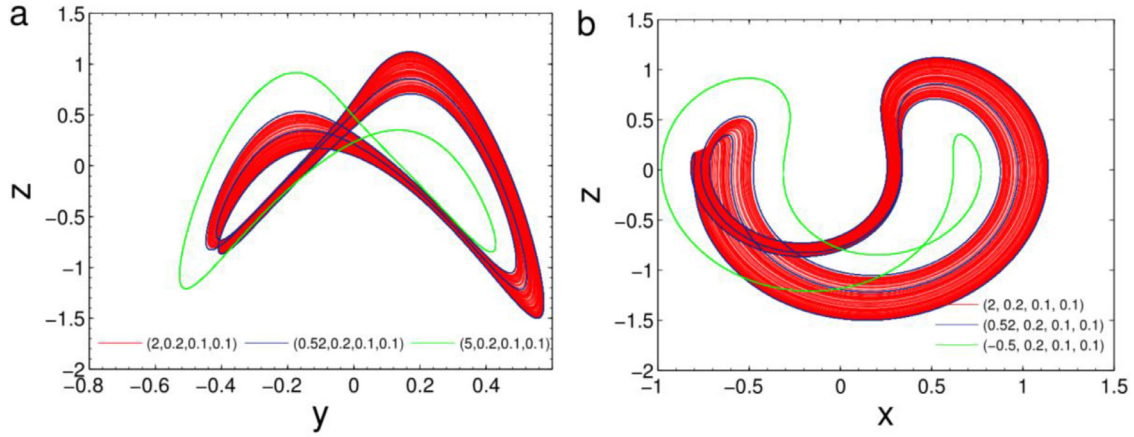

Fig. 12. Three coexisting asymmetric attractors (when $g = 0.03$) in phase plane for $r = 5.39$. period-1 cycle for $IC1 = (5,\ 0.2,\ 0.1,\ 0.1)$, chaotic attractor for $IC2 = (2,\ 0.2,\ 0.1,\ 0.1)$ and period-3 limit cycle for $IC3 = (0.52,\ 0.2,\ 0.1,\ 0.1)$. (a) 2D projection in (y-z) plane, and (b) 2D projection in (x-z) plane.

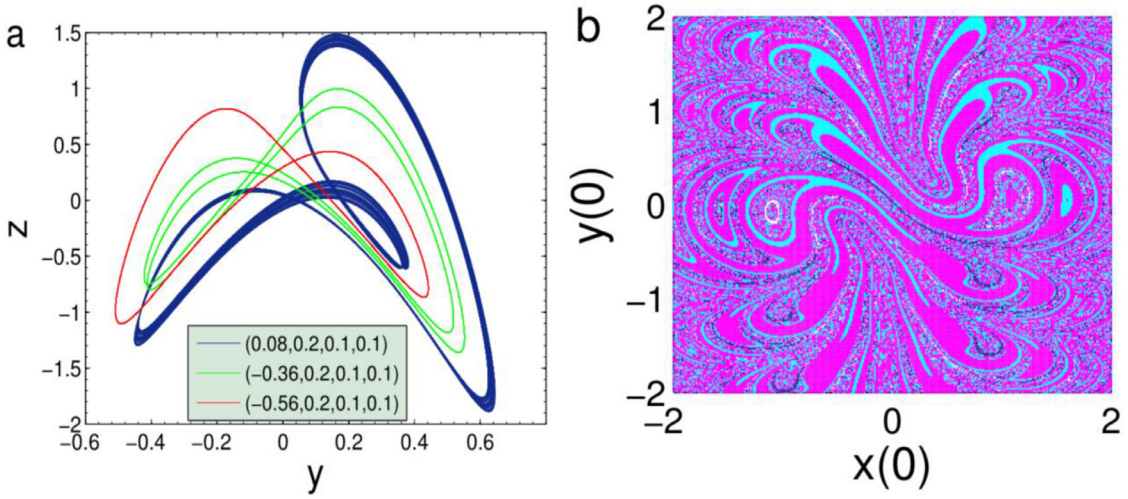

Fig. 13. (a) Coexistence of three asymmetric attractors (when $g = 0.03$, for $r = 5.8$), and (b) corresponding demarcation region of initial points in $(x(0) - y(0))$ plane with $z(0) = u(0) = 0$. A period-1 cycle corresponds to magenta domain, a period-2 cycle for cyan region, and a chaotic attractor for black area. Others parameters are: $\alpha = 1, \beta = 0.05, \gamma = 0.5, m = 11, a = 1$.

of the nonlinear controlled system. To begin, suppose the general form of the nonlinear multistable system $\dot{\zeta} = F(\zeta)$, where ζ is an $m-$dimensional vector of dynamical state, and $F(\zeta)$ represents a vector field. The theory of the LA scheme [16,37,38,61] is through coupling a linear system (ϕ) to a nonlinear one as

$$\begin{cases} \dot{\zeta} = F(\zeta) + \sigma\phi \\ \dot{\phi} = -p\phi - \sigma(\zeta - Q) \end{cases} \tag{17}$$

In the two-dimensional (2D) system (17), σ represents the coupling coefficient between the nonlinear oscillator and the linear control model. The expression $\dot{\phi} = -p\phi$ represents the linear dynamics system coupled to the nonlinear model, and where p is the decay parameter. When there is no coupling (i.e., $\sigma = 0.0$), the linear system is not felt in the whole connected multistable Sprott B system. However, the progressive increase of the coupling coefficient σ allows passing from a region with a large number of coexisting attractors toward another one with a low coexistence of attractors leading to a monostable region for higher coupling values. Next, we construct the new 5D system by coupling the 4D Sprott B system in (2) with the controlled technic described in (17). Indeed, the coupling can be made along with any system's variables. In our case, the coupling is introduced in the third equation (i.e., along the $z-$variable) with the coupling strength σ. The new coupled system is expressed by Eq. (18).

$$\begin{cases} \dot{x} = ryz + g \\ \dot{y} = x - y \\ \dot{z} = 1 - mW(u)xy + \sigma\varphi \\ \dot{u} = axy - u \\ \dot{\varphi} = -p\varphi - \sigma(z - q). \end{cases} \tag{18}$$

Here, $\phi = [0,\ 0,\ \varphi,\ \ldots]^T$ and $Q = [0,\ 0,\ q,\ \ldots]^T$ where T is the transpose. The selection of scalar coupling was guided by recent results of control and synchronization on chaotic systems [38,62]. Indeed, it has been demonstrated that control and synchronization of the chaotic system employing scalars present greater flexibility than the vector. The disadvantage of using vector than scalar for control or synchronization is that the whole states of the systems are affected in the process. This means resources and energy consumption. The results presented in Table 3 show sufficiently that the new 5D coupled Sprott B system has a single unstable equilibrium $E^0 = (x, y, z, u, \varphi)$.

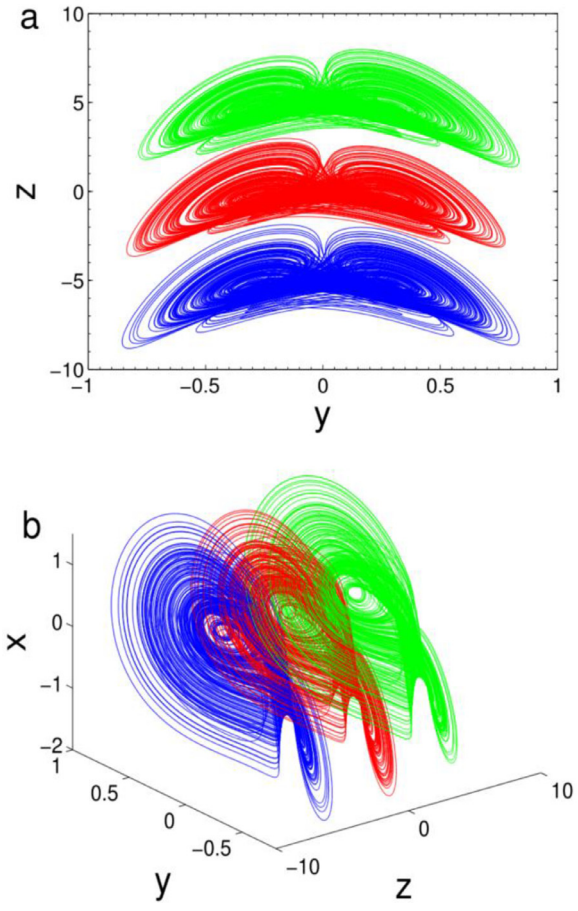

Fig. 14. Offset boosting of the signal in the new memristive system (2) for varying the boostable state δ: red signal for $\delta = 0$, blue signal for $\delta = 5$, and green signal for $\delta = -5$. (a) 2D view in $(y,\ z)$, (b) 3D view in $(z,\ y,\ x)$. The initial point is $(1,\ 0.2,\ 0,\ 0)$, and the rest of the parameters are those in Fig. 1.

This fixed point E^0 given in Eq. (19) is the unique solution of Eq. (21).

$$E^0 = \left[\pm\sqrt{\frac{u}{a}}, \pm\sqrt{\frac{u}{a}},\ -\left(\pm\frac{g}{r}\sqrt{\frac{a}{u}}\right),\ \frac{\sigma}{p}\left(\pm\frac{g}{r}\sqrt{\frac{a}{u}} - q\right), u\right] \tag{19}$$

Table 3
Fixed point E^0 and corresponding eigenvalues for discrete values of the coupling strength σ with $\alpha = 1$, $\beta = 0.05$, $\gamma = 0.5$, $m = 11$, $a = 1$, $r = 4.975$, $p = 0.8$, and $q = 0.7$.

σ	Fixed point E^0	Eigenvalues	Nature of E^0
0.15	(0.29787185, 0.29787185, 0.0, 0.08872764, 0.131250)	$0.3391 \pm 2.4680i$, $-1.6350 + 0.000i$, $-0.7995 + 0.000i$, $-1.0436 + 0.000i$	Unstable saddle-foci
0.6	(0.33627319, 0.33627319, 0.0, 0.11307965, 0.5250)	$0.3443 \pm 2.8135i$, $-1.6384 + 0.000i$, $-0.7941 + 0.000i$, $-1.0560 + 0.000i$	Unstable saddle-foci
1.0	(0.39724878, 0.39724878, 0.0, 0.15780659, 0.8750)	$0.3538 \pm 3.3720i$, $-1.6394 + 0.000i$, $-0.7892 + 0.000i$, $-1.0790 + 0.000i$	Unstable saddle-foci

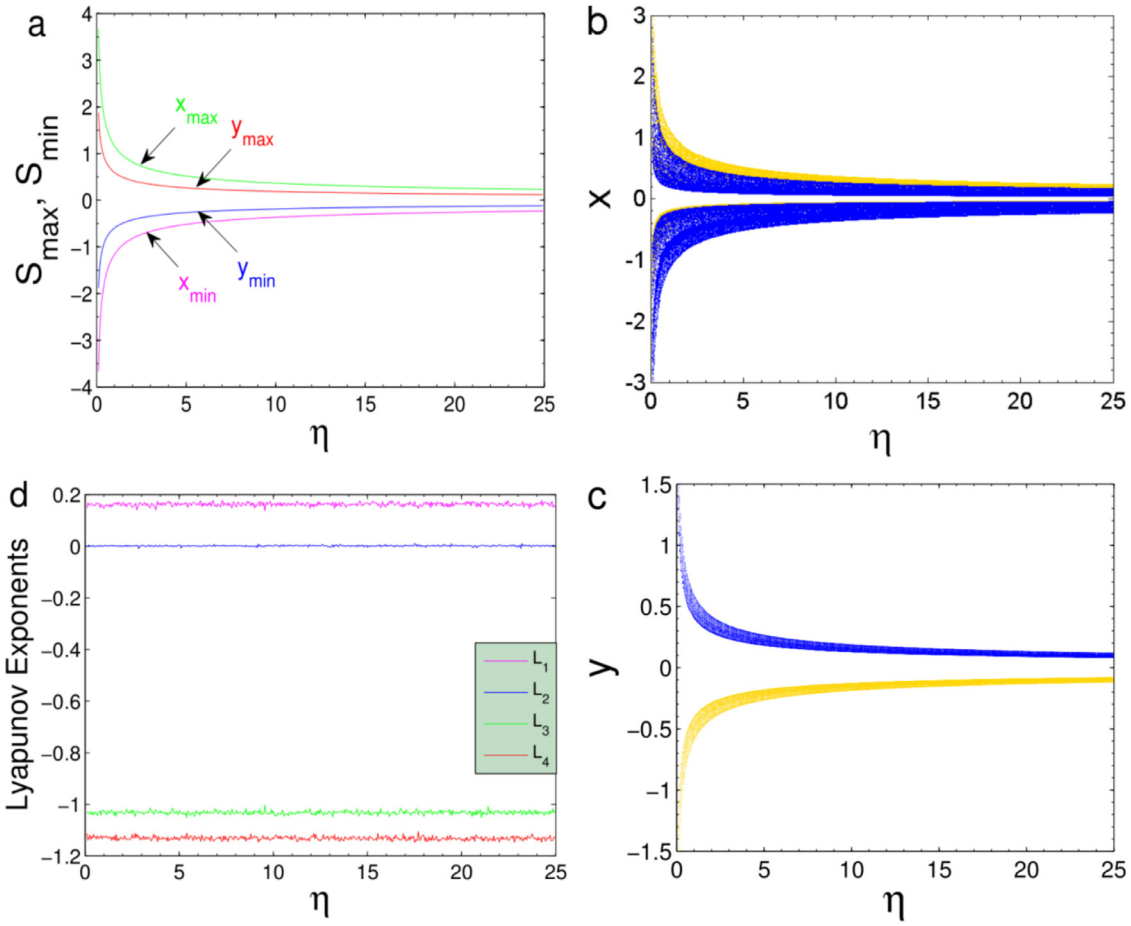

Fig. 15. The signal changing diagram in term of the parameter η evolment in 4D system (16) for $r = 4.7$ in interval $\eta \in [0,\ 25]$. (a) signal amplitude evolvement curve, (b), (c) bifurcation diagrams in the spaces $x - \eta$, and $y - \eta$, (d) Lyapunov exponent spectra. The rest of parameter as well as initial conditions are fixed as in Fig. 6.

where $u$is obtained by solving the transcendental Eq. (20)

$$m\left(\alpha + \gamma|u| + \beta u^2\right)\frac{u}{a} + \frac{\sigma^2}{p}\left(\pm\frac{g}{r}\sqrt{\frac{a}{u}} - q\right) = 1 \tag{20}$$

$$\begin{cases} ryz + g = 0 \\ x - y = 0 \\ 1 - mW(u)xy + \sigma\varphi = 0 \\ axy - u = 0 \\ -p\varphi - \sigma(z - q) = 0 \end{cases} \tag{21}$$

6.2. Results and discussion of linear augmentation control scheme on multistable Sprott B system

In Fig. 17, the linear control strategy implementation results are shown through the coexisting bifurcations branches of the control parameter σ. These coexisting diagrams are obtained by saving the peak values of each state variable and by increasing the coupling strength coefficient σ from 0.0 to 1.0. Indeed, four different ICs are used to gain the coexisting diagrams of Fig. 17 in the same range of parameter σ. The red and yellow branches are obtained using the symmetric $ICs = (\pm 0.4,\ 0,\ 0,\ 0)$, while the branches in green and black are plotted using $ICs = (\pm 0.2,\ 0,\ 0,\ 0)$. When the

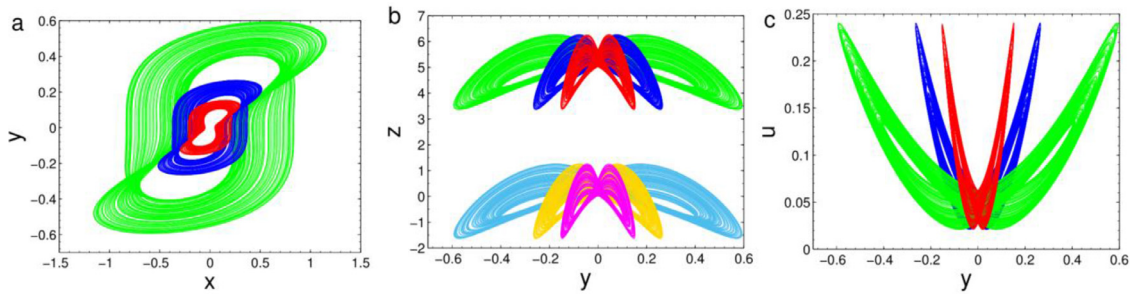

Fig. 16. Partial amplitude control (PAC) of the chaotic signal for varying η in system (16) for $\eta = 1$ (green), $\eta = 5$ (blue), and $\eta = 15$ (red): (a)-(c) controlled phase diagram without offset ($\delta = 0$) in $(x - y)$, and $(y - u)$ planes, (b) controlled phase diagram with offset boosting ($\delta = -5$).

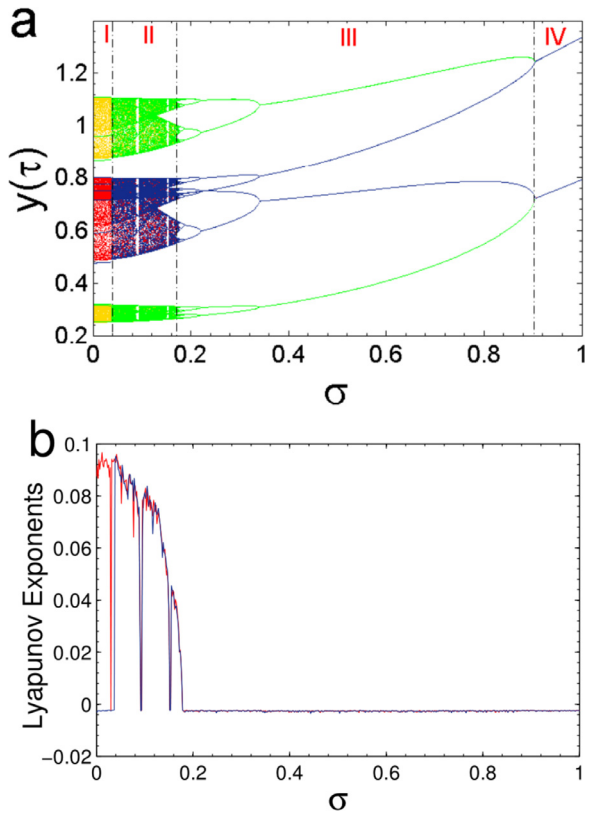

Fig. 17. Maximal Lyapunov exponents (MLE) and corresponding bifurcation diagram of the peak state y showing the evolution of the coupled system (18) when the coupling force σ increase from $_0$ to $_1$. Four different sets of data are superimposed, corresponding to the upward direction values of the control parameter. r was fixed as 4.975 to ensure the four coexisting solutions, as depicted in Fig. 8.

coupling coefficient σ is scanned (i.e., upward direction) in the interval $\sigma\varepsilon[0.0,\ 1.0]$, four attractive regions (namely *I*, *II*, *III*, and *IV*) are observed in the coupled Sprott B system (18). All these interesting dynamics enable the system to move from the multistable areas (with four or two coexisting attractors) to a monostable region with a single surviving periodic attractor. The transition from multistable to monostable dynamics is confirmed through an interior crisis followed by a scenario towards chaos with a reverse period-doubling when σ increases. Demarcation regions of attraction (i.e., the cross-section of the basin of attraction) and 3D phase diagrams are used to confirm this transition, as shown in Fig. 18. Indeed, when the coupling coefficient σ is selected in the region *I* of Fig. 17 (i.e., $\sigma\varepsilon[0.0,\ 4.10^{-2}]$), up to four coexisting solutions are found (see Fig. 18a). For instance, when the coupling coefficient is zero ($\sigma = 0.0$), the demarcation domain of coexisting solutions is distributed in four different colors (see Fig. 18a(i)), resulting in four coexisting solutions in Fig. 18a(ii). After the critical value $\sigma = 4.10^{-2}$ where an interior crisis is viewed, more precisely in the region *II* (i.e., $\sigma\varepsilon]4.10^{-2},\ 16.10^{-2}]$), the green and magenta areas disappear completely (see Fig. 18b(i)), and only a pairs symmetric chaotic attractors coexists as shown in Fig. 18b(ii). In other words, the space magnetization is attracted by two coexisting chaotic solutions. Past the critical value $\sigma = 16.10^{-2}$ (i.e., in the domain $III(\sigma\varepsilon]16.10^{-2},\ 90.10^{-2}[)$), a series of reverse period-doubling is observed until $\sigma \approx 90.10^{-2}$. In this region, we observe the coexistence of solutions pairs with the following sequence $P_m \rightarrow P_8 \rightarrow P_4 \rightarrow P_2$ when σ increases slowly. However, the cross-section of the basin of attraction expands as σ increase but remains confined with two coexisting attractors, as illustrated in Fig. 18c. Next, it is observed from Fig. 18d (particularly in region *IV*) that the pairs coexisting solutions of Fig. 18c (region *III*) merge to form a unique survived symmetric period-1 attractors at the critical value $\sigma = 16.10^{-2}$ where symmetry restoring crisis is observed. The bound area where the survived attractor in the monostable region is plotted for $\sigma = 1.0$.

Similarly, the annihilation process originates the single survived solution of the system can also be demonstrated using the system's control coefficient r for different coupling strengths σ. When the coupling coefficient takes the values $\sigma = 0.0$, $\sigma = 0.18$, $\sigma = 0.4$, and $\sigma = 0.99$, the various bifurcation diagrams of the control parameter r are presented in Fig. 19. The asymmetric bifurcation branch (see Fig. 19d) illustrating the unique survived attractor is obtained for a higher value of σ. Note that the control strategy can be applied in both cases (i.e., for $g = 0.0$ and $g \neq 0.0$). However, to limit the length of the paper, we have chosen one case as a case study. This case corresponds to the regime where the memristive system exhibits four coexisting solutions for the same system's parameters.

7. Discussion and conclusion

This paper proposes a novel 4D memristive chaotic Sprott B system, and its collective nonlinear aspects have been investigated. The introduced model has a bias term that controls the symmetry property of the chaotic oscillator and is therefore responsible for both heterogeneous and homogeneous dynamic behaviors. Using appropriate nonlinear analysis tools like bifurcation diagrams, 2D and 3D phase diagrams, the basin of attractions, Poincaré section, and Lyapunov exponent's spectrum, the collective nonlinear aspects of the new oscillator are uncovered. We correctly prove that pairs of symmetric attractors are emerged/formed in the RS system (i.e., when there is no bias term), and the phenomenon of attractor merging is observed. Also, coexisting symmetric attractors and bifurcations with four solutions are perfectly investigated. However, in the RSB system (i.e., the bias term is different to zero), exciting dynamics/phenomena are found, including asymmetric at-

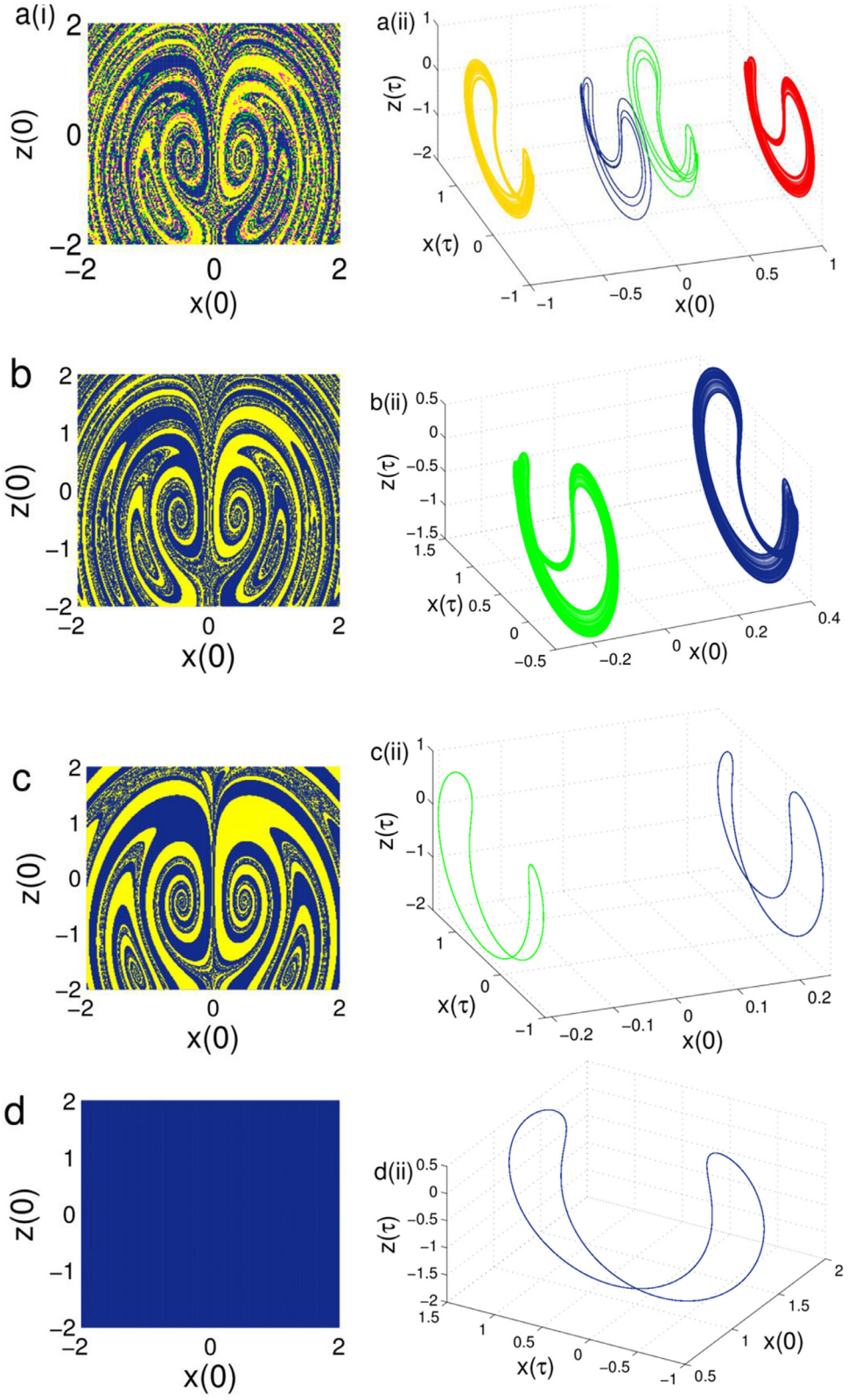

Fig. 18. Space magnetization of the coexisting attractors and corresponding 3D view in the controlled Sprott B system (18). (a) Four coexisting symmetric attractors for $\sigma = 0.0$, (b) pair chaotic attractors for $\sigma = 0.1$, (c) pair symmetric period-2 attractors for $\sigma = 0.8$, and (c) the unique survived period-1 attractor for $\sigma = 1.0$.

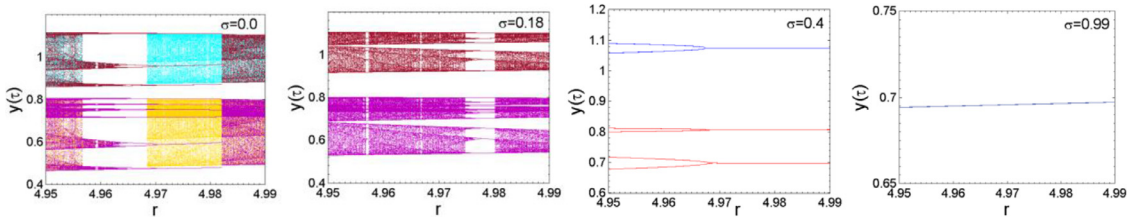

Fig. 19. Bifurcation diagrams of the peak state y vs. the control parameter $r\varepsilon[4.95, 4.99]$ showing the effect of the linear augmented controller on the Sprott B system (2) for distinct values of the coupling force σ. (a) four coexisting branches for $\sigma = 0.0$ obtain in the upward and backward directions (cyan and red when $ICs = (0.5,\ 0, 0, 0, 0)$ and cyan, black branches for $ICs = (\pm 0.5,\ 0, 0, 0, 0)$), (b) two coexisting chaotic branches for $\sigma = 0.18$ (upward and backward directions with $ICs = (0.5,\ 0, 0, 0, 0)$), (d) two coexisting periodic branches for $\sigma = 0.4$ with same ICs, and (e) the unique branch for $\sigma = 0.99$.

tractors, coexisting asymmetric bifurcations, various types of coexisting asymmetric attractors, and period-doubling scenarios. Apart from all these rich dynamics, by investigating the exciting phenomenon of PAC (i.e., partial amplitude control) and offset boosting property, we demonstrate how it is possible to control the amplitude and the offset of the chaotic signals generated for some practical applications.

Moreover, coexisting attractors found in the novel memristive system are further controlled based on a linear augmentation (LA) scheme. Our numerical findings demonstrated the effectiveness of the control technic through interior crisis, reverse period-doubling scenario, and symmetry restoring crisis. The coupled memristive system remains stable with its unique survived periodic attractor for higher values of the coupling strength. All these results sufficiently prove that the objective of this work has been achieved.

Declaration of Competing Interest

The authors declare that they have no known competing financial interests or personal relationships that could have appeared to influence the work reported in this paper.

CRediT authorship contribution statement

Ramesh Ramamoorthy: Formal analysis, Writing – original draft. **Karthikeyan Rajagopal:** Investigation, Conceptualization, Formal analysis, Software. **Gervais Dolvis Leutcho:** Methodology, Conceptualization, Investigation, Writing – review & editing. **Ondrej Krejcar:** Formal analysis, Investigation, Writing – original draft. **Hamidreza Namazi:** Software, Validation, Visualization. **Iqtadar Hussain:** Supervision, Writing – review & editing.

Acknowledgment

This work is partially funded by Center for Nonlinear Systems, Chennai Institute of Technology, India vide funding number CIT/CNS/2021/RD/007. This work was also supported in part by the project (2022/2204), Grant Agency of Excellence, University of Hradec Kralove, Faculty of Informatics and Management, Czech Republic. This work also has been supported by the project of Operational Programme Integrated Infrastructure: Independent research and development of technological kits based on wearable electronics products, as tools for raising hygienic standards in a society exposed to the virus causing the COVID-19 disease, ITMS2014+ code 313011ASK8. Projects are co-funding by European Regional Development Fund.

References

[1] Leutcho GD, Khalaf AJM, Njitacke Tabekoueng Z, Fozin TF, Kengne J, Jafari S, et al. A new oscillator with mega-stability and its Hamilton energy: infinite coexisting hidden and self-excited attractors. Chaos Interdiscip J Nonlinear Sci 2020;30:033112.
[2] Jafari S, Sprott J, Nazarimehr F. Recent new examples of hidden attractors. Eur Phys J Spec Top 2015;224:1469–76.
[3] Kingni ST, Rajagopal K, Tamba VK, Ainamon C, Orou JBC. Analysis and FPGA implementation of an autonomous Josephson junction snap oscillator. Eur Phys J B 2019;92:1–8.
[4] Ren S, Panahi S, Rajagopal K, Akgul A, Pham VT, Jafari S. A new chaotic flow with hidden attractor: the first hyperjerk system with no equilibrium. Z Naturforschung A 2018;73:239–49.
[5] Strukov DB, Snider GS, Stewart DR, Williams RS. The missing memristor found. Nature 2008;453:80–3.
[6] Njitacke Z, Fotsin H, Negou AN, Tchiotsop D. Coexistence of multiple attractors and crisis route to chaos in a novel memristive diode bidge-based Jerk circuit. Chaos Solitons Fractals 2016;91:180–97.
[7] Shaarawy N, Emara A, El-Naggar AM, Elbtity ME, Ghoneima M, Radwan AG. Design and analysis of 2T2M hybrid CMOS-Memristor based RRAM. Microelectron J 2018;73:75–85.
[8] Dong Z, He Y, Hu X, Qi D, Duan S. Flexible memristor-based LUC and its network integration for Boolean logic implementation. IET Nanodielectr 2019;2:61–9.
[9] Lin H, Wang C, Hong Q, Sun Y. A multi-stable memristor and its application in a neural network. IEEE Trans Circuits Syst Express Briefs 2020;67:3472–6.
[10] Noshadian S, Ebrahimzade A, Kazemitabar SJ. Optimizing chaos based image encryption. Multimed Tools Appl 2018;77:25569–90.
[11] Mandal S, Banerjee S. Analysis and CMOS implementation of a chaos-based communication system. IEEE Trans Circuits Syst Regul Pap 2004;51:1708–22.
[12] Zhang J, Zhang C, Feng F, Zhang W, Ma J, Zhang QJ. Polynomial chaos-based approach to yield-driven EM optimization. IEEE Trans Microw Theory Tech 2018;66:3186–99.
[13] Balakrishnan HN, Kathpalia A, Saha S, Nagaraj N. ChaosNet: a chaos based artificial neural network architecture for classification. Chaos Interdiscip J Nonlinear Sci 2019;29:113125.
[14] Cicek I, Pusane AE, Dundar G. A novel design method for discrete time chaos based true random number generators. Integration 2014;47:38–47.
[15] Nestor T, De Dieu NJ, Jacques K, Yves EJ, Iliyasu AM, El-Latif A, et al. A multidimensional hyperjerk oscillator: dynamics analysis, analogue and embedded systems implementation, and its application as a cryptosystem. Sensors 2020;20:83.
[16] Njitacke ZT, Sone ME, Fozin TF, Tsafack N, Leutcho GD, Tchapga CT. Control of multistability with selection of chaotic attractor: application to image encryption. Eur Phys J Spec Top 2021;230:1839–54.
[17] Abd EL-Latif AA, Abd-El-Atty B, Venegas-Andraca SE, Mazurczyk W. Efficient quantum-based security protocols for information sharing and data protection in 5 G networks. Future Gener. Comput Syst 2019;100:893–906.
[18] Abd EL-Latif AA, Abd-El-Atty B, Abou-Nassar EM, Venegas-Andraca SE. Controlled alternate quantum walks based privacy preserving healthcare images in internet of things. Opt Laser Technol 2020;124:105942.
[19] Li C, Sprott JC. Coexisting hidden attractors in a 4-D simplified Lorenz system. Int J Bifurc. Chaos 2014;24:1450034.
[20] Lai Q, Kamdem Kuate PD, Pei H, Fotsin H. Infinitely many coexisting attractors in no-equilibrium chaotic system. Complexity 2020;2020:1–17.
[21] Wan Q, Zhou Z, Ji W, Wang C, Yu F. Dynamic analysis and circuit realization of a novel no-equilibrium 5D memristive hyperchaotic system with hidden extreme multistability. Complexity 2020;2020:1–16.
[22] Zhou L, Chen Z, Wang J, Zhang Q. Local bifurcation analysis and global dynamics estimation of a novel 4-dimensional hyperchaotic system. Int J Bifurc Chaos 2017;27:1750021.
[23] Ojoniyi OS, Njah AN. A 5D hyperchaotic Sprott B system with coexisting hidden attractors. Chaos Solitons Fractals 2016;87:172–81.
[24] Xiaoxia L, Xue W, Zhixin F, Qiyu Z. Dynamics analysis and circuit realization of Sprott-B hyper-chaotic system based on memristor. Chin J Quantum Electron 2021;38:393.
[25] Zhang S, Zheng J, Wang X, Zeng Z. A novel no-equilibrium HR neuron model with hidden homogeneous extreme multistability. Chaos Solitons Fractals 2021;145:110761.
[26] Chen M, Ren X, Wu HG, Xu Q, Bao BC. Periodically varied initial offset boosting behaviors in a memristive system with cosine memductance. Front Inf Technol Electron Eng 2019;20:1706–16.

[27] Bao B, Bao H, Wang N, Chen M, Xu Q. Hidden extreme multistability in memristive hyperchaotic system. Chaos Solitons Fractals 2017;94:102–11.
[28] Bao BC, Xu Q, Bao H, Chen M. Extreme multistability in a memristive circuit. Electron Lett 2016;52:1008–10.
[29] Kengne J, Leutcho GD, Telem ANK. Reversals of period doubling, coexisting multiple attractors, and offset boosting in a novel memristive diode bridge-based hyperjerk circuit. Analog Integr Circuits Signal Process 2018;101:379–99.
[30] Kengne LK, Pone JRM, Fotsin HB. On the dynamics of chaotic circuits based on memristive diode-bridge with variable symmetry: a case study. Chaos Solitons Fractals 2021;145:110795.
[31] Zang H, Gu Z, Lei T, Li C, Jafari S. Coexisting chaotic attractors in a memristive system and their amplitude control. Pramana 2020;94:1–9.
[32] Xu Q, Cheng S, Ju Z, Chen M, Wu H. Asymmetric coexisting bifurcations and multi-stability in an asymmetric memristive diode-bridge-based Jerk circuit. Chin J Phys 2021;70:69–81.
[33] Sprott JC. Some simple chaotic flows. Phys Rev E 1994;50:R647.
[34] Li C, Thio WJC, Sprott JC, Iu HHC, Xu Y. Constructing infinitely many attractors in a programmable chaotic circuit. IEEE Access 2018;6:29003–12.
[35] Tabekoueng Njitacke Z, Sami Doubla I, Kengne J, Cheukem A. Coexistence of firing patterns and its control in two neurons coupled through an asymmetric electrical synapse. Chaos Interdiscip J Nonlinear Sci 2020;30:023101.
[36] Njitacke ZT, Isaac SD, Nestor T, Kengne J. Window of multistability and its control in a simple 3D hopfield neural network: application to biomedical image encryption. Neural Comput Appl 2021;33:6733–52.
[37] Fonzin Fozin T, Megavarna Ezhilarasu P, Njitacke Tabekoueng Z, Leutcho G, Kengne J, Thamilmaran K, et al. On the dynamics of a simplified canonical Chua's oscillator with smooth hyperbolic sine nonlinearity: hyperchaos, multistability and multistability control. Chaos Interdiscip J Nonlinear Sci 2019;29:113105.
[38] Leutcho GD, Kengne J, Fonzin Fozin T, Srinivasan K, Njitacke Tabekoueng Z, Jafari S, et al. Multistability control of space magnetization in hyperjerk oscillator: a case study. J Comput Nonlinear Dyn 2020;15(5):051004.
[39] Sharma PR, Shrimali MD, Prasad A, Kuznetsov NV, Leonov GA. Controlling dynamics of hidden attractors. Int J Bifurc Chaos 2015;25:1550061.
[40] Yadav K, Kamal NK, Shrimali MD. Intermittent feedback induces attractor selection. Phys Rev E 2017;95:042215.
[41] Lai Q, Wan Z, Kamdem Kuate PD, Fotsin H. Dynamical analysis, circuit implementation and synchronization of a new memristive hyperchaotic system with coexisting attractors. Mod Phys Lett B 2021;35:2150187.
[42] Lai Q, Wan Z, Kengne LK, Kuate PDK, Chen C. Two-memristor-based chaotic system with infinite coexisting attractors. IEEE Trans Circuits Syst Express Briefs 2020;68:2197–201.
[43] Ma S, Zhou P, Ma J, Wang C. Phase synchronization of memristive systems by using saturation gain method. Int J Mod Phys B 2020;34:2050074.
[44] Meli MIT, Yemélé D, Leutcho GD. Dynamical analysis of series hybrid electric vehicle powertrain with torsional vibration: antimonotonicity and coexisting attractors. Chaos Solitons Fractals 2021;150:111174.
[45] Tametang Meli MI, Leutcho GD, Yemele D. Multistability analysis and nonlinear vibration for generator set in series hybrid electric vehicle through electromechanical coupling. Chaos Interdiscip J Nonlinear Sci 2021;31:073126.
[46] Lai Q, Norouzi B, Liu F. Dynamic analysis, circuit realization, control design and image encryption application of an extended Lü system with coexisting attractors. Chaos Solitons Fractals 2018;114:230–45.
[47] Wei Z, Zhang W. Hidden hyperchaotic attractors in a modified Lorenz–Stenflo system with only one stable equilibrium. Int J Bifurc Chaos 2014;24:1450127.
[48] Wei Z, Wang R, Liu A. A new finding of the existence of hidden hyperchaotic attractors with no equilibria. Math Comput Simul 2014;100:13–23.
[49] Leutcho G, Kengne J, Kengne LK. Dynamical analysis of a novel autonomous 4-D hyperjerk circuit with hyperbolic sine nonlinearity: chaos, antimonotonicity and a plethora of coexisting attractors. Chaos Solitons Fractals 2018;107:67–87.
[50] Leutcho GD, Kengne J, Kengne LK, Akgul A, Pham VT, Jafari S. A novel chaotic hyperjerk circuit with bubbles of bifurcation: mixed-mode bursting oscillations, multistability, and circuit realization. Phys Scr 2020;95:075216.
[51] Leutcho GD, Wang H, Kengne R, Kengne LK, Njitacke ZT, Fozin TF. Symmetry-breaking, amplitude control and constant Lyapunov exponent based on single parameter snap flows. Eur Phys J Spec Top 2021;230:1887–903.
[52] Abd el-Latif AA, Abd-el-Atty B, Amin M, Iliyasu AM. Quantum-inspired cascaded discrete-time quantum walks with induced chaotic dynamics and cryptographic applications. Sci Rep 2020;10:1–16.
[53] Tsafack N, Sankar S, Abd-El-Atty B, Kengne J, Jithin K, Belazi A, et al. A new chaotic map with dynamic analysis and encryption application in internet of health things. IEEE Access 2020;8:137731–44.
[54] Li C, Sprott JC. Variable-boostable chaotic flows. Optik 2016;127:10389–98 (Stuttg).
[55] Li C, Lei T, Wang X, Chen G. Dynamics editing based on offset boosting. Chaos Interdiscip J Nonlinear Sci 2020;30:063124.
[56] Gu J, Li C, Chen Y, Iu HH, Lei T. A conditional symmetric memristive system with infinitely many chaotic attractors. IEEE Access 2020;8:12394–401.
[57] Lai Q, Kuate PDK, Liu F, Iu HHC. An extremely simple chaotic system with infinitely many coexisting attractors. IEEE Trans Circuits Syst Express Briefs 2019;67(6):1129–33.
[58] Li C, Sprott J. Finding coexisting attractors using amplitude control. Nonlinear Dyn 2014;78:2059–64.
[59] Li C, Sprott JC, Yuan Z, Li H. Constructing chaotic systems with total amplitude control. Int J Bifurc Chaos 2015;25:1530025.
[60] Li CB, Wang HK, Chen S. A novel chaotic attractor with constant Lyapunov exponent spectrum and its circuit implementation. 2010.
[61] Sharma P, Shrimali M, Prasad A, Kuznetsov N, Leonov G. Control of multistability in hidden attractors. Eur Phys J Spec Top 2015;224:1485–91.
[62] Lian KY, Liu P, Chiang TS, Chiu CS. Adaptive synchronization design for chaotic systems via a scalar driving signal. IEEE Trans Circuits Syst I Fundam Theory Appl 2002;49:17–27.